How to cite: *Angew. Chem. Int. Ed.* **2021**, *60*, 26357–26362
International Edition: doi.org/10.1002/anie.202110829
German Edition: doi.org/10.1002/ange.202110829

Functional Self-Assembly

Versatile Polymer Nanocapsules via Redox Competition

*Jiajing Zhou, Ming Xu, Zhicheng Jin, Raina M. Borum, Nicole Avakyan, Yong Cheng, Wonjun Yim, Tengyu He, Jingcheng Zhou, Zhuohong Wu, Yash Mantri, and Jesse V. Jokerst**

Abstract: *Polymer nanocapsules have demonstrated significant value in materials science and biomedical technology, but require complicated and time-consuming synthetic steps. We report here the facile synthesis of monodisperse polymer nanocapsules via a redox-mediated kinetic strategy from two simple molecules: dopamine and benzene-1,4-dithiol (BDT). Specifically, BDT forms core templates and modulates the oxidation kinetics of dopamine into polydopamine (PDA) shells. These uniform nanoparticles can be tuned between ≈ 70 and 200 nm because the core diameter directly depends on BDT while the shell thickness depends on dopamine. The supramolecular core can then rapidly disassemble in organic solvents to produce PDA nanocapsules. Such nanocapsules exhibit enhanced physicochemical performance (e.g., loading capacity, photothermal transduction, and anti-oxidation) versus their solid counterparts. Particularly, this method enables a straightforward encapsulation of functional nanoparticles providing opportunities for designing complex nanostructures such as yolk–shell nanoparticles.*

Hollow nanocapsules have been widely synthesized for biomedicine, energy storage, and catalysis because they provide a functional void for cargo loading and an increasingly reactive interface area.[1–5] Polymer nanocapsules with engineered size and surface chemistry are a prominent type of capsule that have been used as a viable drug delivery system and diagnostic probe due to their excellent biocompatibility.[6,7] However, their compelling potential is often bottlenecked by limitations in synthesis. Pre-synthesized uniform templates (e.g., polymer, silica, and metal nanoparticles) are commonly adopted for such nanocapsules,[8–12] but these templates require tedious and elaborate shell fabrication (e.g., layer-by-layer or surface-initiated polymerization) and possible harsh template removal (e.g., etchant treatment).[13–16] While emulsion-mediated nanocapsule synthesis has been developed to streamline these synthetic pathways, the method's size control—such as over structural parameters and size distribution—remains challenging.[17,18] Alternative efforts have created special polymers or ligands that can self-assemble into nanocapsules in the absence of templates.[19–21] These template-free strategies transfer the complicated steps to polymer synthesis and/or assembly process rather than streamline the nanocapsule fabrication. Thus, a simple method that produces tunable and uniform polymer nanocapsules could dramatically extend the trajectory of polymer nanocapsules for a variety of applications, especially in biomedicine.

Polydopamine (PDA) is inspired by the mussel adhesive protein and has good biocompatibility and excellent adhesive properties on diverse substrates.[22–24] The polymerization of dopamine typically occurs in an alkaline environment in the presence of oxidizers (e.g., oxygen, metal ions): dopamine-o-quinone and dihydroxyindole are produced to subsequently form PDA complexes.[25,26] The catechol groups present in PDA further enable their versatile and facile conjugation with surface ligands via the Michael addition or Schiff base reactions.[27] Consequently, PDA-based nanomaterials—especially nanocapsules—have been extensively used for biomedical applications such as drug delivery (e.g., anti-cancer drug, protein, and gene), diagnostics (e.g., magnetic resonance imaging and photoacoustic imaging), and therapy (e.g., photothermal and photodynamic therapy) as well as advanced bio-nano fundamentals.[28–30] In this context, immense efforts have been dedicated to expedite the process of PDA to nanoparticle formation equilibrium, substrate coating, or matrix crosslinking. These steps are thus critical performance indicators in this field.[31–36] Somewhat surprisingly, a counterintuitive method that *retards* the polymerization of dopamine into PDA rather than accelerates it is rarely investigated.

We report here a redox-mediated kinetic strategy to synthesize uniform PDA nanocapsules by using two simple molecules: dopamine and benzene-1,4-dithiol (BDT). In a typical synthesis, BDT is mixed with dopamine in a basic environment. BDT undergoes preferential oxidation into polymerized BDT (PBDT) due to the lower redox potential compared to dopamine, and the resulting PBDT can assemble into a supramolecular PBDT core.[37,38] When the BDT is depleted, dopamine oxidizes into PDA resulting in a PDA coating on the pre-formed PBDT cores (Figure 1 and S1).

[*] Dr. J. Zhou, Dr. M. Xu, Dr. Z. Jin, R. M. Borum, Dr. Y. Cheng, Dr. J. Zhou, Z. Wu, Prof. J. V. Jokerst
Department of NanoEngineering, University of California San Diego
9500 Gilman Drive, La Jolla, CA 92093 (USA)
E-mail: jjokerst@eng.ucsd.edu
Dr. N. Avakyan
Department of Chemistry and Biochemistry, University of California San Diego
9500 Gilman Drive, La Jolla, California 92093 (USA)
W. Yim, T. He, Prof. J. V. Jokerst
Materials Science and Engineering Program, University of California San Diego
9500 Gilman Drive, La Jolla, California 92093 (USA)
Y. Mantri
Department of Bioengineering, University of California San Diego
9500 Gilman Drive, La Jolla, California 92093 (USA)
Prof. J. V. Jokerst
Department of Radiology, University of California San Diego
9500 Gilman Drive, La Jolla, California 92093 (USA)
Supporting information and the ORCID identification number(s) for the author(s) of this article can be found under: https://doi.org/10.1002/anie.202110829.

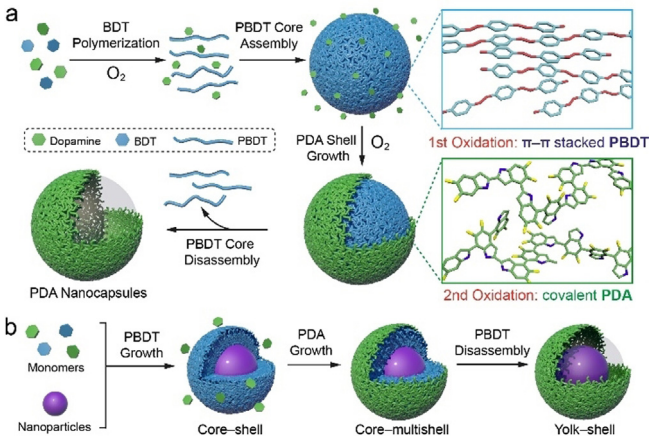

Figure 1. Redox-mediated pathway to synthesize core–shell and nanocapsule nanostructures (a) and yolk–shell nanostructures (b). The surfactant (i.e., sodium dodecyl sulfate) is not shown in the Scheme for simplicity. The sequential oxidation of the monomers plays a key role in this strategy.

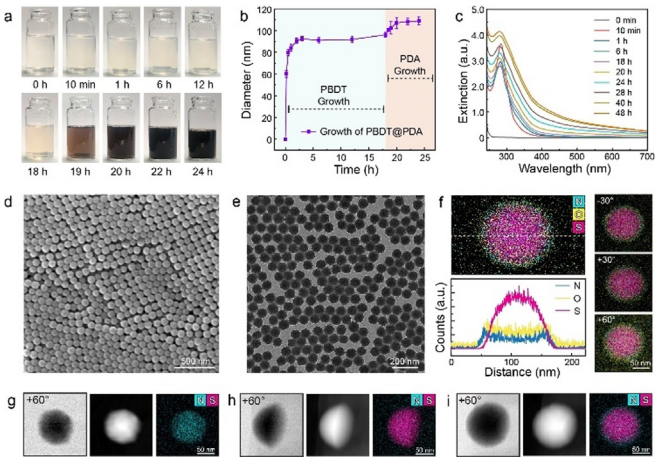

Figure 2. Dynamic growth of PBDT@PDA core–shell nanoparticles. a) Photos of the reaction solution at different time points. b) Time-dependent hydrodynamic size of the PBDT@PDA nanoparticles during the growth process. c) Time-dependent UV/Vis spectra of PBDT@PDA nanoparticles during the growth process. d) SEM image of PBDT@PDA nanoparticles. e) TEM image of the PBDT@PDA nanoparticles. f) Elemental mapping of the PBDT@PDA nanoparticles at different tilting angles and its representative line scanning profile. g–i) Bright field TEM, HAADF, and EDX images of a representative PDA (g), PBDT (h), and PBDT@PDA (i) nanoparticle at a tilting angle of +60°.

Particularly, the core size of the nanoparticles can be tuned from 50 to more than 100 nm by adjusting the concentration of BDT while the shell thickness can be tuned from 10 to more than 70 nm by adjusting the amount of dopamine. Removing the supramolecular PBDT core from the PBDT@PDA core–shell nanoparticles in organic solvents further produced uniform PDA nanocapsules. The kinetic growth of core–shell nanoparticles and their assembly/disassembly behavior are investigated. We show that PDA nanocapsules have outstanding loading capacity, high photothermal conversion efficiency, photoacoustic signal, and antioxidation performance. This redox-mediated strategy not only creates diverse functional polymer nanocapsules, but also enables facile integration of nanoparticles for multifunctional PDA nanocapsules (i.e., yolk–shell structures).

The uniform PBDT@PDA core–shell nanoparticles were prepared by mixing BDT (0.2 mg mL^{-1}) and dopamine (0.4 mg mL^{-1}) in TRIS buffer (10 mM, pH 8.5). The reaction solution remained colorless in the first 12 h (Figure 2a), and dynamic light scattering (DLS) indicated the formation of nanoparticles ($\approx$90 nm) in solution (Figure 2b). These results collectively demonstrate the formation of PBDT nanoparticles and negligible formation of PDA complexes, thus implying the inhibited polymerization of dopamine. This is consistent with the redox potentials of phenol (E_{pa} = + 0.484 V) and thiol groups (E_{pa} = + 0.330 V) suggesting that BDT is more prone to donate its electrons for oxidation.[39] The color of the solution was light yellow in the first 18 h and turned dark brown relatively quickly (i.e., from 18 to 22 h). This remains in agreement with the resumed nanoparticle growth in the DLS results.

UV/Vis spectra further demonstrated increased absorbance from 350 to 700 nm after 18 h (Figure 2c) validating the formation of brown PDA.[40] To elucidate the competing oxidation between thiol and catechol, we mixed monothiol-containing molecules and a non-thiol molecule with dopamine in the buffer (Figure S2). The results indicate that thiol moieties significantly inhibit the oxidation of dopamine (Figure S3,4). Therefore, we can infer that the oxidation of BDT into PBDT cores occurs first in the mixture, which in turn can modulate the polymerization kinetics of dopamine.

Scanning electron microscopy (SEM) and transmission electron microscopy (TEM) images showed monodisperse spherical PBDT@PDA nanoparticles after 24 h of reaction (Figure 2d,e). Three-dimensional TEM and energy dispersive X-ray (EDX) tomography validated the presence of two "immiscible" components in PBDT@PDA nanoparticles, where PBDT (represented by S) comprised the core and PDA (represented by N) formed the shell (Figure 2f). It is notable that while PDA is a rigid polymer (Figure 2g),[41] PBDT is a soft material that can easily deform after drying on the TEM grids (Figure 2h). Therefore, the obtained PDA shell can maintain the complete sphere morphology of the PBDT core (Figure 2i) compared to mono-component PDA or PBDT nanoparticles (Figure 2g–i and S5–8).

We then investigated the size tunability of these core–shell nanoparticles by varying the concentration of precursors (i.e., dopamine and BDT) and surfactant (i.e., sodium dodecyl sulfate, SDS). The key findings are summarized as follows (Figure 3a and S9): Increasing the concentration of dopamine or BDT produces larger nanoparticles, but increasing the concentration of surfactant produces smaller nanoparticles. When the concentration of BDT was raised from 100 to 300 μg mL^{-1}, the overall size of the core–shell system was modulated from 80 to 160 nm. We conclude that SDS plays a crucial role in controlling the size over a relatively wide range (70 to 200 nm) (Figure S9). Specifically, more surfactants can compensate the higher surface energy to render smaller nanoparticles.[11,42]

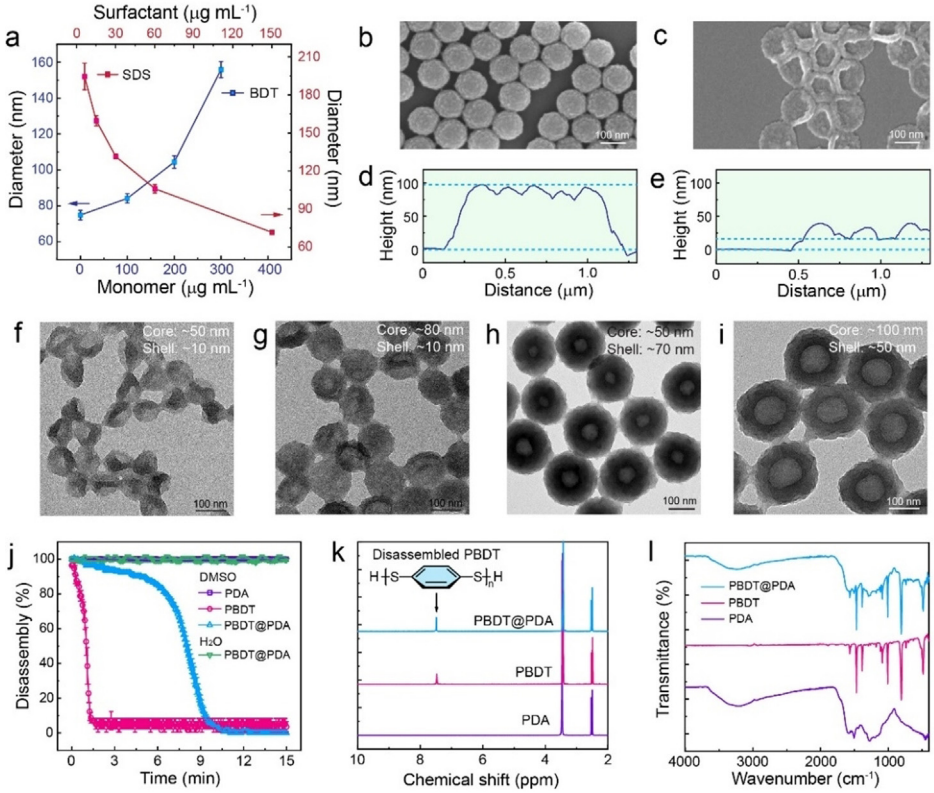

Figure 3. Transformation of core–shell nanostructures into nanocapsules. a) DLS results for PBDT@PDA core–shell nanoparticles prepared by varying the concentration of BDT (400 μg mL^{-1} dopamine and 60 μg mL^{-1} SDS) and surfactant (200 μg mL^{-1} BDT and 400 μg mL^{-1} dopamine). b,c) SEM images of representative PBDT@PDA nanoparticles (core 80 nm and shell 10 nm) before and after core removal in DMSO. d,e) AFM height profiles of PBDT@PDA before (d) and after (e) core removal. f–i) Various nanocapsules derived from core–shell nanoparticles. j) Disassembly kinetics of different nanoparticles via monitoring their scattering intensities. k) ^{1}H NMR (300 MHz, [D$_6$]DMSO, 298 K) data of PDA, PBDT, and PBDT@PDA nanoparticles. l) FTIR spectra of different nanoparticles.

While the PBDT nanoparticles are primarily stabilized by π-π interactions, the formation of PDA is dominated by robust covalent interactions.[43,44] Therefore, we hypothesized that the supramolecular PBDT nanoparticles would be removed during the solvent treatment to produce uniform PDA nanocapsules.[45] This is corroborated by incubating the core–shell nanoparticles in dimethyl sulfoxide (DMSO) for 15 min: SEM and atomic force microscopy (AFM) demonstrated the transformation of core–shell nanoparticles into crumpled nanocapsules via DMSO (Figure 3b–e and S10,11). By using different core–shell nanoparticles, a series of nanocapsules with different shell thicknesses (e.g., from ≈10 to 70 nm) and cavities (e.g., from ≈50 to 100 nm) were prepared (Figure 3 f–j and S10). It is notable that thicker PDA shells retain the complete spherical cavity of the nanocapsules, while the thinner ones collapse into crumpled structures after drying (Figure 3 f,h).

To gain more insights into the assembly/disassembly process, a comparison study between PDA nanoparticles, PBDT nanoparticles, and PBDT@PDA core–shell nanoparticles was implemented. All three nanoparticles showed good stability in aqueous environments. While the covalent crosslinking nature of PDA allowed it to maintain the colloidal structure in DMSO, PBDT showed rapid disassembly in DMSO in 2 min as the light scattering of PBDT significantly diminished (Figure 3j). In contrast, PBDT@PDA nanoparticles showed a slower disassembly kinetic for PBDT mainly due to the presence of PDA shells, which retards the diffusion of DMSO and the disassembly of PBDT in the core. Of particular interest, nuclear magnetic resonance (NMR) confirmed the disassembly of PBDT after incubation with DMSO (Figure 3k and S12). Neither PDA nor PBDT showed characteristic NMR signal of the aromatic region in D_2O due to the densely crosslinked or packed nature of these polymers.

In deuterated DMSO ([D$_6$]DMSO), PBDT disassembled and exhibited a chemical shift at 7.48 ppm. This peak was also observed in the sample of PBDT@PDA nanoparticles suggesting the release of free PBDT from the PDA shells. Thermogravimetric analysis (TGA) indicated the polymeric nature of the obtained PBDT@PDA nanoparticles due to the improved thermal stability (Figure S13). Moreover, Fourier-transform infrared spectroscopy (FTIR) confirmed the presence of phase-segregated PDA and PBDT components in the PBDT@PDA (Figure 3l).

We then explored the potential applications of PDA nanocapsules compared to PDA nanoparticles, PBDT nanoparticles, and PBDT@PDA core–shell nanoparticles. The cargo loading capacity of these nanoparticles was evaluated first. It is notable that PBDT nanoparticles have negligible

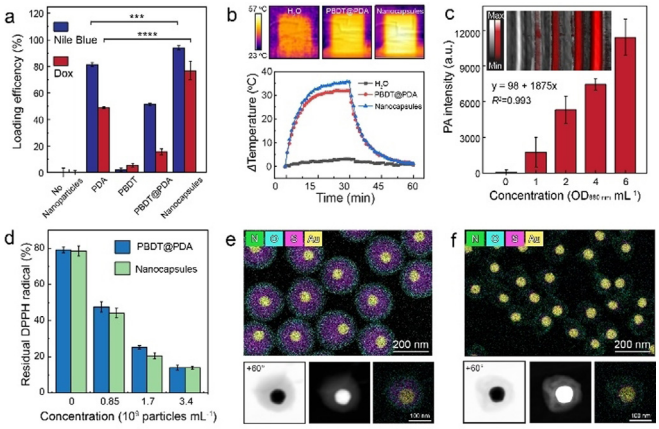

Figure 4. Functional and structural versability of PDA nanocapsules. a) Loading efficiency of different nanoparticles towards Nile blue A and Dox. The error bars represent standard deviations ($n=3$). b) Photothermal performance of PBDT@PDA nanoparticles and PDA nanocapsules. The optical density is 1.0 at 808 nm. c) Concentration-dependent photoacoustic performance of PDA nanocapsules. The error bars represent the standard deviations calculated from different regions of interest ($n=6$). d) Antioxidant activities of nanoparticles and nanocapsules as evaluated by a DPPH assay. The error bars represent standard deviations ($n=3$). e) Elemental mapping of Au@PBDT@PDA and its corresponding bright-field TEM, HAADF, and EDX images at a tilting angle of +60°. f) Elemental mapping of Au@PDA yolk–shell nanoparticles and its corresponding bright field TEM, HAADF, and EDX images at a tilting angle of +60°.

capacity to load either Nile blue A or doxorubicin (Dox). PDA nanoparticles, however, showed a higher loading efficiency (e.g., 48.9% for DOX) compared to PBDT (5.4%) and PBDT@PDA (15.6%) nanoparticles at the same mass concentration (400 $\mu g\,mL^{-1}$) (Figure 4a) because the catechol-rich PDA possesses high affinity to those aromatic cargos due to π-π interactions and electrostatic interactions.[46,47] Moreover, PDA nanocapsules showed the highest loading efficiency amongst all the nanoparticle systems including PDA nanoparticles due to the advantage of hollow structures (i.e., 12.3% increase for Nile blue A and 27.1% increase for Dox versus PDA nanoparticles).[48]

Melanin-like PDA has a broad absorbance from the UV/Vis to the near-infrared (NIR) range, and has therefore been widely used as a photo-mediated theranostic agent.[49] In this context, we investigated different photo-thermal properties of these new nanocapsules. Upon NIR light irradiation (i.e., 808 nm laser), the PDA nanocapsules showed improved photothermal transduction (52.0%) compared to the solid PBDT@PDA nanoparticles (43.2%) (Figure 4b and S14). Meanwhile, the photoacoustic performance, where pulsed laser irradiation induces the pressure transients to produce ultrasound signals, was also studied.[50] PDA nanoparticles exhibited 1.2-fold PA enhancement over PBDT@PDA core–shell nanoparticles at the same mass concentration (500 $\mu g\,mL^{-1}$) while PDA nanocapsules of same optical density (at 680 nm) showed more than 2-fold PA enhancement over PBDT@PDA core–shell nanoparticles (Figure S15 and S16). This can be ascribed to the reduced scattering contribution in the overall extinction of PDA nanocapsules. The optical density-dependent PA property of those PDA nanocapsules was further summarized (Figure 4c), indicating their potential as PA contrast agents.

Phenolics have been recognized as antioxidants.[51] We therefore evaluated the antioxidation performance of different nanoparticle systems using a 2,2-diphenyl-1-picrylhydrazyl (DPPH) assay (Figure S17). Intriguingly, both dopamine and BDT showed good anti-oxidation properties due to the catechol groups in dopamine and the thiol groups in BDT (Figure S18). While PDA nanoparticles maintained anti-oxidation properties, PBDT nanoparticles completely lost such reactivity (Figure S18). This suggests extensive consumption of thiol groups in BDT and/or highly dense packing of PBDT in nanoparticles. To compare the antioxidant properties between nanoparticles and nanocapsules, we benchmarked their nanoparticle concentration (e.g., 10^9 particles mL^{-1}) using nanoparticle tracking analysis (Figure S19–21). The results demonstrated that PDA nanocapsules possess slightly faster antioxidation kinetics compared to PBDT@PDA nanoparticles (Figure 4d and S22) due to the increased PDA surface area available for scavenging $DPPH^{\cdot}$ radicals.

We further demonstrated that this redox-mediated kinetic strategy accommodates the streamlined integration of functional cores into these capsules for yolk–shell nanoparticles (Figure S23). For example, when 60 nm gold nanoparticles (AuNPs) were co-mixed with the dopamine and BDT monomers, well-defined Au core and multi-shell (i.e., PBDT inner layer and PDA outermost layer) nanostructures were obtained. EDX confirmed the two distinct shell materials on Au nanoparticles (Figure 4e and S24). After incubating the nanoparticles in DMSO for 15 min, the PBDT intermediate layer disassembled and yolk–shell nanoparticles were formed (Figure 4f and S25). Distinct yolk–shell nanoparticles can be synthesized by varying the concentrations of dopamine and BDT (Figure S26,27). Combined with the low toxicity of PBDT and PDA, the facile strategy for yolk–shell nanoparticle synthesis shows potentials for designing diverse multifunctional nanostructures for biomedical applications (Figure S28).[28,52]

We reported a simple, robust, and versatile method to prepare uniform polymer nanocapsules with tunable shell thickness and cavity diameter as well as optional functional cores. This method relies on the competing oxidation of BDT and dopamine where BDT first polymerizes into PBDT followed by subsequent polymerization of dopamine into PDA. The π-π stabilized PBDT cores can selectively disassemble in organic solvent within minutes to produce PDA nanocapsules. This redox-mediated synthesis can produce PDA nanocapsules with improved drug loading capacity as well as anti-oxidative and light-responsive properties. It can also facilitate the formation of complex yolk–shell nanostructures. We envision that this strategy offers new opportunities for emerging applications for phenolic-enabled nanotechnology and biomedicine.

Acknowledgements

This work was performed in part at the San Diego Nanotechnology Infrastructure (SDNI) of University of California San Diego, a member of the National Nanotechnology Coordinated Infrastructure (NNCI), Which is supported by the National Science Foundation (Grant ECCS-1542148). The authors acknowledge the use of facilities and instrumentation supported by NSF through the UC San Diego Materials Research Science and Engineering Center (UCSD MRSEC) (Grant DMR-2011924). R.M.B. acknowledges support from the National Cancer Institute of the National Institutes of Health under the award number T32 CA153915. N.A. acknowledges support from NSF (DMR-2004558). J.V.J. acknowledges funding from NIH under DP2 HL137187, S10 OD021821, and S10 OD023555, as well as NSF 1845683.

Conflict of Interest

The authors declare no conflict of interest.

Keywords: functional self-assembly · nanocapsules · polydopamine · supramolecular chemistry · theranostic probes

[1] F. Wu, C. Pan, C. T. He, Y. H. Han, W. J. Ma, H. Wei, W. L. Ji, W. X. Chen, J. J. Mao, P. Yu, D. S. Wang, L. Q. Mao, Y. D. Li, *J. Am. Chem. Soc.* **2020**, *142*, 16861 – 16867.
[2] X. Q. Hu, M. R. Han, L. Shao, C. Zhang, L. Zhang, S. P. Kelley, C. Zhang, J. Lin, S. J. Dalgarno, D. A. Atwood, S. S. Feng, J. L. Atwood, *Angew. Chem. Int. Ed.* **2021**, *60*, 10516 – 10520; *Angew. Chem.* **2021**, *133*, 10610 – 10614.
[3] C. B. Gao, F. L. Lyu, Y. D. Yin, *Chem. Rev.* **2021**, *121*, 834 – 881.
[4] T. Bollhorst, K. Rezwan, M. Maas, *Chem. Soc. Rev.* **2017**, *46*, 2091 – 2126.
[5] Z. J. Chen, S. C. Yang, X. L. Liu, Y. H. Gao, X. Dong, X. Lai, M. H. Zhu, H. Y. Feng, X. D. Zhu, Q. Lu, M. Zhao, H. Z. Chen, J. F. Lovell, C. Fang, *Nano Lett.* **2020**, *20*, 4177 – 4187.
[6] X. Gong, R. M. Li, J. Wang, J. Wei, K. Ma, X. Q. Liu, F. Wang, *Angew. Chem. Int. Ed.* **2020**, *59*, 21648 – 21655; *Angew. Chem.* **2020**, *132*, 21832 – 21839.
[7] E. Golub, R. H. Subramanian, J. Esselborn, R. G. Alberstein, J. B. Bailey, J. A. Chiong, X. D. Yan, T. Booth, T. S. Baker, F. A. Tezcan, *Nature* **2020**, *578*, 172 – 176.
[8] Y. Y. Han, Z. X. Lin, J. J. Zhou, G. Yun, R. Guo, J. J. Richardson, F. Caruso, *Angew. Chem. Int. Ed.* **2020**, *59*, 15618 – 15625; *Angew. Chem.* **2020**, *132*, 15748 – 15755.
[9] J. Q. Chen, J. H. Li, J. J. Zhou, Z. X. Lin, F. Cavalieri, E. Czuba-Wojnilowicz, Y. J. Hu, A. Glab, Y. Ju, J. J. Richardson, F. Caruso, *ACS Nano* **2019**, *13*, 11653 – 11664.
[10] J. C. Qiu, D. Huo, J. J. Xue, G. H. Zhu, H. Liu, Y. N. Xia, *Angew. Chem. Int. Ed.* **2019**, *58*, 10606 – 10611; *Angew. Chem.* **2019**, *131*, 10716 – 10721.
[11] J. J. Zhou, Z. X. Lin, M. Penna, S. J. Pan, Y. Ju, S. Y. Li, Y. Y. Han, J. Q. Chen, G. Lin, J. J. Richardson, I. Yarovsky, F. Caruso, *Nat. Commun.* **2020**, *11*, 4804.
[12] Y. J. Liu, J. L. Wang, M. Y. Zhang, H. M. Li, Z. J. Lin, *ACS Nano* **2020**, *14*, 12491 – 12521.
[13] J. J. Richardson, M. Bjornmalm, F. Caruso, *Science* **2015**, *348*, aaa2491.
[14] J. O. Zoppe, N. C. Ataman, P. Mocny, J. Wang, J. Moraes, H. A. Klok, *Chem. Rev.* **2017**, *117*, 1105 – 1318.
[15] Z. Zeng, M. F. Wen, G. Ye, X. M. Huo, F. C. Wu, Z. Wang, J. J. Yang, K. Matyjaszewski, Y. X. Lu, J. Chen, *Chem. Mater.* **2017**, *29*, 10212 – 10219.
[16] S. T. Gunawan, K. Kempe, T. Bonnard, J. W. Cui, K. Alt, L. S. Law, X. W. Wang, E. Westein, G. K. Such, K. Peter, C. E. Hagemeyer, F. Caruso, *Adv. Mater.* **2015**, *27*, 5153 – 5157.
[17] X. B. Yan, M. Delgado, A. Fu, P. Alcouffe, S. G. Gouin, E. Fleury, J. L. Katz, F. Ganachaud, J. Bernard, *Angew. Chem. Int. Ed.* **2014**, *53*, 6910 – 6913; *Angew. Chem.* **2014**, *126*, 7030 – 7033.
[18] M. Ma, H. X. Xu, H. R. Chen, X. Q. Jia, K. Zhang, Q. Wang, S. G. Zheng, R. Wu, M. H. Yao, X. J. Cai, F. Q. Li, J. L. Shi, *Adv. Mater.* **2014**, *26*, 7378 – 7385.
[19] A. K. Khan, S. Gudlur, H. P. M. de Hoog, W. Siti, B. Liedberg, M. Nallani, *Angew. Chem. Int. Ed.* **2017**, *56*, 11754 – 11758; *Angew. Chem.* **2017**, *129*, 11916 – 11920.
[20] Y. N. Liu, H. Wang, S. L. Li, C. S. Chen, L. Xu, P. Huang, F. Liu, Y. Su, M. W. Qi, C. Y. Yu, Y. F. Zhou, *Nat. Commun.* **2020**, *11*, 1724.
[21] B. P. Bastakoti, J. Perez-Mercader, *Angew. Chem. Int. Ed.* **2017**, *56*, 12086 – 12091; *Angew. Chem.* **2017**, *129*, 12254 – 12259.
[22] H. Lee, S. M. Dellatore, W. M. Miller, P. B. Messersmith, *Science* **2007**, *318*, 426 – 430.
[23] Y. L. Liu, K. L. Ai, L. H. Lu, *Chem. Rev.* **2014**, *114*, 5057 – 5115.
[24] H. A. Lee, E. Park, H. Lee, *Adv. Mater.* **2020**, *32*, 1907505.
[25] C. Zhang, Y. Ou, W. X. Lei, L. S. Wan, J. Ji, Z. K. Xu, *Angew. Chem. Int. Ed.* **2016**, *55*, 3054 – 3057; *Angew. Chem.* **2016**, *128*, 3106 – 3109.
[26] H. C. Yang, Q. Y. Wu, L. S. Wan, Z. K. Xu, *Chem. Commun.* **2013**, *49*, 10522 – 10524.
[27] P. Yang, F. Zhu, Z. B. Zhang, Y. Y. Cheng, Z. Wang, Y. W. Li, *Chem. Soc. Rev.* **2021**, *50*, 8319 – 8343.
[28] D. Wu, J. Zhou, M. N. Creyer, W. Yim, Z. Chen, P. B. Messersmith, J. V. Jokerst, *Chem. Soc. Rev.* **2021**, *50*, 4432 – 4483.
[29] Y. Z. Sun, E. Davis, *Langmuir* **2020**, *36*, 9333 – 9342.
[30] D. R. Amin, C. J. Higginson, A. B. Korpusik, A. R. Gonthier, P. B. Messersmith, *ACS Appl. Mater. Interfaces* **2018**, *10*, 34792 – 34801.
[31] Y. Wang, E. J. Jeon, J. Lee, H. Hwang, S. W. Cho, H. Lee, *Adv. Mater.* **2020**, *32*, 2002118.
[32] B. D. B. Tiu, P. Delparastan, M. R. Ney, M. Gerst, P. B. Messersmith, *Angew. Chem. Int. Ed.* **2020**, *59*, 16616 – 16624; *Angew. Chem.* **2020**, *132*, 16759 – 16767.
[33] J. W. Li, M. A. Baird, M. A. Davis, W. Y. Tai, L. S. Zweifel, K. M. A. Waldorf, M. Gale, L. Rajagopal, R. H. Pierce, X. H. Gao, *Nat. Biomed. Eng.* **2017**, *1*, 0082.
[34] C. Zhang, B. H. Wu, Y. S. Zhou, F. Zhou, W. M. Liu, Z. K. Wang, *Chem. Soc. Rev.* **2020**, *49*, 3605 – 3637.
[35] J. H. Lee, J. S. Ryu, Y. K. Kang, H. Lee, H. J. Chung, *Adv. Funct. Mater.* **2021**, *31*, 2170056.
[36] J. W. Li, T. Wang, A. R. Kirtane, Y. H. Shi, A. Jones, Z. Moussa, A. Lopes, J. Collins, S. M. Tamang, K. Hess, R. Shakur, P. Karandikar, J. S. Lee, H. W. Huang, A. Hayward, G. Traverso, *Sci. Transl. Med.* **2020**, *12*, eabc0441.
[37] B. Liu, M. A. Beatty, C. G. Pappas, K. Liu, J. Ottele, S. Otto, *Angew. Chem. Int. Ed.* **2021**, *60*, 13569 – 13573; *Angew. Chem.* **2021**, *133*, 13681 – 13685.
[38] J. Zhou, M. N. Creyer, A. Chen, W. Yim, R. P. M. Lafleur, T. He, Z. Lin, M. Xu, P. Abbasi, J. Wu, T. A. Pascal, F. Caruso, J. V. Jokerst, *J. Am. Chem. Soc.* **2021**, *143*, 12138 – 12144.
[39] D. Chavarria, C. Fernandes, T. Silva, J. Garrido, F. Remiao, P. J. Oliveira, F. Borges, *Org. Biomol. Chem.* **2019**, *17*, 9646 – 9654.
[40] Y. Zou, X. F. Chen, P. Yang, G. J. Liang, Y. Yang, Z. P. Gu, Y. W. Li, *Sci. Adv.* **2020**, *6*, eabb4696.
[41] J. J. Zhou, C. X. Wang, P. Wang, P. B. Messersmith, H. W. Duan, *Chem. Mater.* **2015**, *27*, 3071 – 3076.
[42] J. M. Jung, G. Savin, M. Pouzot, C. Schmitt, R. Mezzenga, *Biomacromolecules* **2008**, *9*, 2477 – 2486.

[43] Z. E. Siwicka, F. A. Son, C. Battistella, M. H. Moore, J. Korpanty, N. C. McCallum, Z. Wang, B. J. Johnson, O. K. Farha, N. C. Gianneschi, *J. Am. Chem. Soc.* **2021**, *143*, 3094 – 3103.
[44] J. Zhou, M. Penna, Z. Lin, Y. Han, R. P. M. Lafleur, Y. Qu, J. J. Richardson, I. Yarovsky, J. V. Jokerst, F. Caruso, *Angew. Chem. Int. Ed.* **2021**, *60*, 20225 – 20230; *Angew. Chem.* **2021**, *60*, 20225 – 20230.
[45] M. F. J. Mabesoone, A. R. A. Palmans, E. W. Meijer, *J. Am. Chem. Soc.* **2020**, *142*, 19781 – 19798.
[46] H. C. Gao, Y. M. Sun, J. J. Zhou, R. Xu, H. W. Duan, *ACS Appl. Mater. Interfaces* **2013**, *5*, 425 – 432.
[47] Z. X. Wang, H. C. Yang, F. He, S. Q. Peng, Y. X. Li, L. Shao, S. B. Darling, *Matter* **2019**, *1*, 115 – 155.
[48] J. Cui, Y. Yan, G. K. Such, K. Liang, C. J. Ochs, A. Postma, F. Caruso, *Biomacromolecules* **2012**, *13*, 2225 – 2228.
[49] W. J. Yim, J. J. Zhou, Y. Mantri, M. N. Creyer, C. A. Moore, J. V. Jokerst, *ACS Appl. Mater. Interfaces* **2021**, *13*, 14974 – 14984.
[50] Y. Mantri, J. V. Jokerst, *ACS Nano* **2020**, *14*, 9408 – 9422.
[51] X. F. Bao, J. H. Zhao, J. Sun, M. Hu, X. R. Yang, *ACS Nano* **2018**, *12*, 8882 – 8892.
[52] W. T. Wang, H. Mattoussi, *Acc. Chem. Res.* **2020**, *53*, 1124 – 1138.

Manuscript received: August 12, 2021
Accepted manuscript online: September 27, 2021
Version of record online: November 5, 2021

